Electronic π-delocalization Boosts Catalytic Water Oxidation by Cu(II) Molecular Catalysts Heterogenized on Graphene Sheets

Pablo Garrido-Barros,[a,b] Carolina Gimbert-Suriñach,[a] Dooshaye Moonshiram,[a] Antonio Picón,[c,d] Pere Monge,[a] Victor S. Batista,[e,*] and Antoni Llobet[a,f,*]

[a] Institute of Chemical Research of Catalonia (ICIQ), Avinguda Països Catalans 16, 43007 Tarragona, Spain

[b] Departament de Química Física i Inorga`nica, Universitat Rovira i Virgili, Campus Sescelades, C/Marcel·lí Domingo, s/n, 43007, Tarragona, Spain

[c] Grupo de Investigación en Aplicaciones del Láser y Fotónica, Departamento de Física Aplicada, Universidad de Salamanca, 37008, Salamanca, Spain.

[d] ICFO—Institut de Ciencies Fotoniques, The Barcelona Institute of Science and Technology, 08860 Castelldefels, Barcelona, Spain.

[e] Department of Chemistry, Yale University. P.O. Box 208107, New Haven, CT 06520-8107, USA

[f] Departament de Química, Universitat Auto`noma de Barcelona, 08193 Cerdanyola del Vallès, Barcelona, Spain.

Supporting Information Placeholder

ABSTRACT: A molecular water oxidation catalyst based on the copper complex of general formula $[(L_{py})Cu^{II}]^{2-}$, $\mathbf{2}^{2-}$, (L_{py} is 4-pyrenyl-1,2-phenylenebis(oxamidate) ligand) has been rationally designed and prepared to support a more extended π-conjugation through its structure in contrast with its homologue, the $[(L)Cu^{II}]^{2-}$ water oxidation catalyst, $\mathbf{1}^{2-}$ (L is o-phenylenebis(oxamidate)). The catalytic performance of both catalysts has been comparatively studied in homogeneous phase and in heterogeneous phase by π-stacking anchorage to graphene-based electrodes. In the homogeneous system, the electronic perturbation provided by the pyrene functionality translates into a 150 mV lower overpotential for $\mathbf{2}^{2-}$ respect to $\mathbf{1}^{2-}$ and an impressive increase in the k_{cat} from 6 s^{-1} to 128 s^{-1}. Upon anchorage, π-stacking interactions with the graphene sheets provide further π-delocalization that improves the catalytic performance of both catalysts. In this sense, $\mathbf{2}^{2-}$ turned out to be the most active catalyst due to the double influence of both the pyrene and the graphene, displaying an overpotential of 538 mV, a k_{cat} of 540 s^{-1} and producing more than 5300 TONs.

Heterogenized water-oxidation catalysis based on earth abundant transition metals, such as Mn, Fe, Co, Ni and Cu, are highly desired for sustainable energy technologies that exploit direct solar water-splitting.[1] An advantage of heterogenized homogeneous catalysts, when compared to heterogeneous catalysts,[2] is that they can be improved by ligand design. Yet first-row transition metal complexes pose several challenges. They usually get deactivated when immobilized on electrode surfaces and they suffer from instability due to hydrolytic behavior and decomposition into metal-oxides upon oxidation of the organic ligands.[3] However, from an engineering perspective, solid-state electroanodes are desired due to the simplicity of assembly for potential devices. Therefore, it is imperative to understand the influence of the anchoring functionality on the performance of the immobilized catalysts to learn how to anchor and stabilize functional molecular catalysts on electrode surfaces.[4,5] Here, we focus on water oxidation by Cu(II) molecular catalysts heterogenized on graphene surfaces.

A family of copper complexes based on tetraamide ligands, such as $[(L)Cu^{II}]^{2-}$, $\mathbf{1}^{2-}$, (L = *o*-phenylenebis(oxamidate)) shown in Figure 1, have been recently reported to be effective at catalyzing oxygen evolution by water oxidation at basic pH.[6] Remarkably, the rate determining step (rds) was found to involve reversible oxidation of the phenyl ring. Here, we explore whether the catalytic properties of these complexes can be manipulated by electronic perturbation of the tetraamide π-system, either by modification of the ligand or by π-stacking to graphitic electrode surfaces.

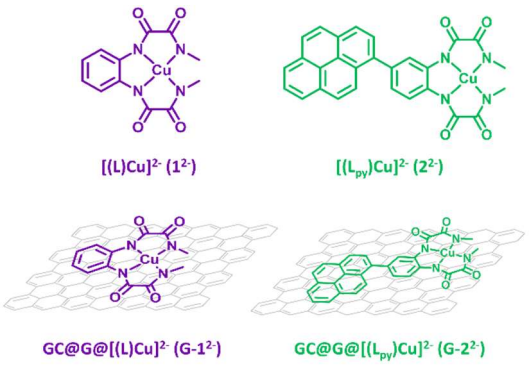

Figure 1. Structural representation and labeling code of the complexes and the hybrid materials used in this work.

We focus on complex $\mathbf{1}^{2-}$ as well as on the analogous catalyst $[(L_{py})Cu^{II}]^{2-}$, $\mathbf{2}^{2-}$ with the 4-pyrenyl-1,2-phenylenebis(oxamidate) ligand $(L_{py})^{4-}$ that has extended π-conjugation via a pyrene moiety covalently connected to the phenyl ring (see SI for a detailed synthetic description) (see Figure 1). We analyze the water oxidation catalytic performance both in the homogeneous phase and heterogenized on graphene sheets. The pyrene anchoring functionality is ideally suited for the comparative analysis since it allows for strong attachment to graphitic surfaces with molecular-surface interactions that are not as much affected by the supporting electrolyte as in the case of oxo-acid type of functionalities.[7]

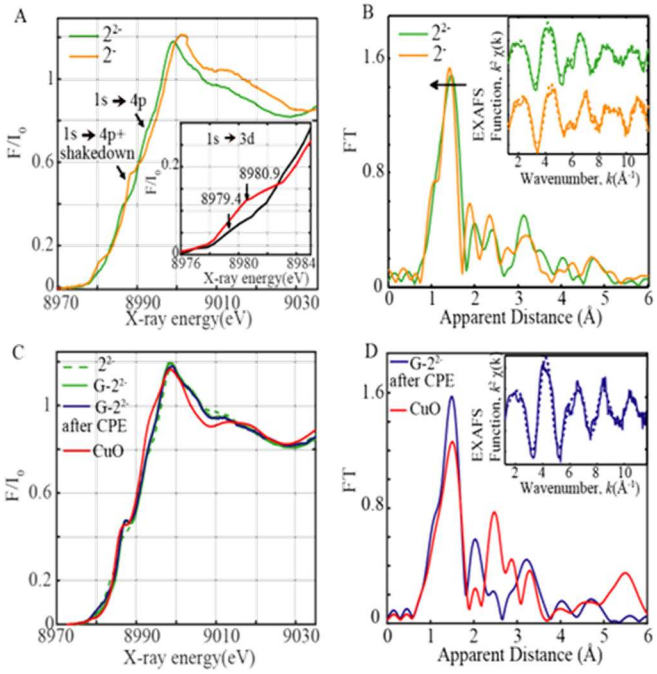

Figure 2. A, Normalized Cu K-edge XANES of $\mathbf{2}^{2-}$ and $\mathbf{2}^{-}$ in MeCN. Inset: zoom-in of the pre-edge regions. **B**, Experimental Fourier transforms of k²-weighted Cu EXAFS of $\mathbf{2}^{2-}$ and $\mathbf{2}^{-}$in MeCN. Inset. Back Fourier transforms, experimental results (solid lines), and fitting (dashed lines) $k^2\,\chi(k)$ for $\mathbf{2}^{2-}$ and $\mathbf{2}^{-}$ in MeCN. Experimental spectra were calculated for k values of 1.212 to 11.6 Å^{-1}. **C**, Normalized Cu K-edge XANES of $\mathbf{2}^{2-}$, $\mathbf{G\text{-}2}^{2-}$, $\mathbf{G\text{-}2}^{2-}$ after controlled potential electrolysis (CPE) at 1.25 V and CuO. **D**, Experimental Fourier transforms of k²-weighted Cu EXAFS of $\mathbf{G\text{-}2}^{2-}$ after CPE and CuO. Inset: Back Fourier transforms, experimental results (solid lines), and fitting (dashed lines) $k^2\,\chi(k)$ for $\mathbf{G\text{-}2}^{2-}$ after CPE. Experimental spectra were calculated for k values of 1.212 to 11.6 Å^{-1}.

The synthesis of complex $[(L_{py})Cu^{II}]^{2-}$, $\mathbf{2}^{2-}$, is straightforward (as described in the SI). We characterized complex $\mathbf{2}^{2-}$ and its one electron oxidized homologue $[(L_{py})Cu^{III}]^{-}$, $\mathbf{2}^{-}$, by using analytic, spectroscopic and electrochemical techniques as well as DFT calculations. Furthermore, MeCN frozen solutions of $\mathbf{2}^{2-}$ and $\mathbf{2}^{-}$ (potentiometrically prepared) were studied by X-ray absorption near edge structure (XANES) (Figure 2A) and extended X-ray absorption fine structure (EXAFS) spectroscopy (Figure 2B). Cu K-edge XANES were generally characterized by two peaks along the rising maximum edge, namely the 1s → 4p main transition along with a 1s → (4p+shakedown) transition, assigned as the 1s → 4p transition with concurrent ligand to metal charge transfer (LMCT), as illustrated in Figure 2A and S14.[8] The XANES spectrum of $\mathbf{2}^{-}$ relative to $\mathbf{2}^{2-}$ shows a clear edge energy shift of 1.5 eV at around half height and 0.65 normalized absorption, reflecting the higher ionization energy required for ejecting a core 1s electron from a more positively charged ion. The distinct metal-centered oxidation of $\mathbf{2}^{-}$ *vs.* $\mathbf{2}^{2-}$ is shown by the 1.5 eV energy shift in the pre-edge energy range from 8979.4 to 8980.9 eV, corresponding to the 1s → 3d electronic transition (Figure 2A, S16, Table S1). Moreover, the 1s → (4p+shakedown) transition is strikingly more intense than the 1s → 4p main transition in $\mathbf{2}^{-}$ than in $\mathbf{2}^{2-}$as illustrated by XANES K-edge fits (Figure S16), providing another indication for the oxidation of Cu(II) to Cu(III) as previously demonstrated by Solomon and co-workers and X-ray photoelectron studies carried out on Cu(II) and Cu(III) oxides.[9,10] The EXAFS spectra (Figure 2B) further revealed a prominent peak in the first coordination sphere corresponding to the Cu-N bond distances. Analysis of the first peak resolves the Cu-N distances for $\mathbf{2}^{2-}$ and $\mathbf{2}^{-}$ to be 1.93 Å and 1.86 Å respectively, in agreement with the calculated relaxed structures from DFT geometry optimization and typical shortened Cu-N/O bond lengths expected for oxidized Cu(III) species (Table S2, S3, Figure S17). Cu K-edge EXAFS for $\mathbf{1}^{2-}$ and $\mathbf{1}^{-}$ in MeCN solutions were also carried out under identical experimental conditions and yielded similar Cu-N bond distances and similar 1.54 eV energy edge shift at half height in the XANES spectra as $\mathbf{2}^{2-}$ and $\mathbf{2}^{-}$ respectively (Table S2, S3, Figure S18). Interestingly, however, a decreased intensity in the pre-edge features of both $\mathbf{1}^{2-}$ and $\mathbf{1}^{-}$ compared to $\mathbf{2}^{2-}$ and $\mathbf{2}^{-}$ was observed, most likely due to the more rigorous centrosymmetric environment displayed by $\mathbf{1}^{2-}$ and $\mathbf{1}^{-}$ (Figure S16 A).[11]

The UV-vis spectra for $\mathbf{2}^{2-}$ and $\mathbf{2}^{-}$ both in MeCN and in aqueous solution at pH = 12, are depicted in Figure 3A. The corresponding spectra of $\mathbf{1}^{2-}$ and $\mathbf{1}^{-}$ are provided in the SI. The Cu(III) spectrum of $\mathbf{2}^{-}$ in MeCN is characterized by a small hypsochromic shift with regard to that of Cu(II) in $\mathbf{2}^{2-}$. In sharp contrast, the spectrum of $\mathbf{2}^{-}$ in aqueous solution is characterized by a drastic decrease of the intensity of the bands at 340 nm. This is consistent with the fact that the first oxidation process occurs at the pyrene moiety[12] rather than at the Cu center in aqueous solution. This striking difference is associated with the increase in π-delocalization due to the pyrene functionalized ligand, L_{py}, that significantly lowers the oxidation potential at the ligand site[13] together with the large stabilization to the putatively charged oxidized species in the aqueous environment.

Figures 3B-3D provide further support for π-delocalization as manifested by the redox properties of the complexes. Figure 3B shows the CVs of $\mathbf{1}^{2-}$ and $\mathbf{2}^{2-}$ at pH = 12. The anodic scanning of $\mathbf{1}^{2-}$ exhibits a first wave at 0.56 V *vs.* NHE, as-

signed to the Cu(III)/Cu(II) couple.[14] A sharp increase in current density at around 1.2 V is associated with the electrocatalytic oxidation of water to dioxygen, after formation of the radical cation $[(L^{+})Cu^{III}(OH)]^{-}$. The first oxidation wave of $\mathbf{2}^{2-}$ is cathodically shifted by 130 mV due to the pyrene oxidation. This ligand-based oxidation was further confirmed by electrochemical means on a homologue $[(L_{py})Zn]^{2-}$ complex, since Zn is a redox non-active metal (See SI Figure S22). The electrocatalytic wave is also cathodically shifted by approximately 150 mV. In this case, the oxidation occurs first at the ligand and subsequently at the metal center, concomitant with OH^{-} coordination, as supported by DFT calculations of the complete catalytic cycle (Scheme 1). Analogous to the mechanism of $\mathbf{1}^{2-}$, the rate-determining step involves ET transfer to generate $[(L_{py^{+}})Cu^{III}(OH)]^{-}$.

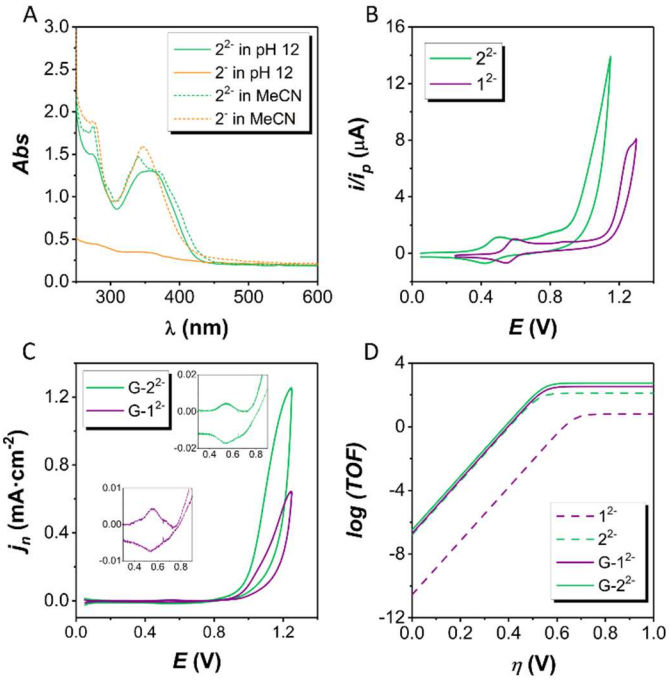

Figure 3. **A**, UV-vis spectra for $\mathbf{2}^{2-}$and $\mathbf{2}^{-}$ in MeCN and in aqueous solution at pH = 12. **B**, CV of $\mathbf{1}^{2-}$ and $\mathbf{2}^{2-}$. **C**, Background corrected CV of **G-1**$^{2-}$ and **G-2**$^{2-}$. Inset shows an enlargement of the 0.2-1.0 V potential range. **D**, Tafel plots for $\mathbf{1}^{2-}$, $\mathbf{2}^{2-}$, **G-1**$^{2-}$ and **G-2**$^{2-}$.

The foot of the wave analysis (FOWA) was carried out to further characterize the electrocatalytic phenomenon,[15,16] giving a maximum turn over frequency (TOF_{max}) of 6.2 s^{-1} for $\mathbf{1}^{2-}$. In sharp contrast to $\mathbf{2}^{2-}$, the TOF_{max} increases up to 128 s^{-1} under the same conditions, manifesting the strong influence of π-delocalization over catalysis.

Complexes $\mathbf{1}^{2-}$ and $\mathbf{2}^{2-}$ were anchored to graphene by preparing a dispersion of 1 mg of graphene (**G**) per mL of a methanol solution containing 1 mM $\mathbf{1}^{2-}$ or $\mathbf{2}^{2-}$. The dispersion was stirred overnight at RT to afford a modified graphene material which was subsequently drop casted into glassy carbon (GC) electrodes. The resulting preparative procedure generated hybrid materials **GC@G@1**$^{2-}$ (**G-1**$^{2-}$) and **GC@G@2**$^{2-}$ (**G-2**$^{2-}$) with surface coverages of 0.052 nmol/cm² and 0.050 nmol/cm² respectively, as measured from CV experiments (see SI). The anchored species were characterized by XANES and EXAFS, and were found to have similar bond distances and XANES features as those obtained in MeCN frozen solutions of the individual molecules (Figure 2C and the SI). It is interesting to note that the 1s → 4p (+shakedown) transition at 8987 eV and 0.5 normalized fluorescence of the immobilized **G-2**$^{2-}$ complex is found at a slightly higher energy and intensity than the corresponding transition for homogeneous $\mathbf{2}^{2-}$. Further, the CVs of the anchored catalysts displayed in Figure 3C, show a first oxidation wave at 0.52 V and a huge catalytic wave associated with the oxidation of water to dioxygen basically at nearly the same overpotential (η) as in the case of $\mathbf{2}^{2-}$ in the homogenous phase. The 100 mV anodic shift of the first oxidation couple in heterogeneous phase with respect to $\mathbf{2}^{2-}$ (0.53 V *vs*. 0.43 V) is due to the lower degree of solvent stabilization of the anion radical cation in contact with the hydrophobic surface of graphene. A FOWA analysis was again carried out to quantify the electrocatalytic rates obtaining TOF_{max} of 320 s^{-1} and 540 s^{-1} for **G-1**$^{2-}$ and **G-2**$^{2-}$, respectively.

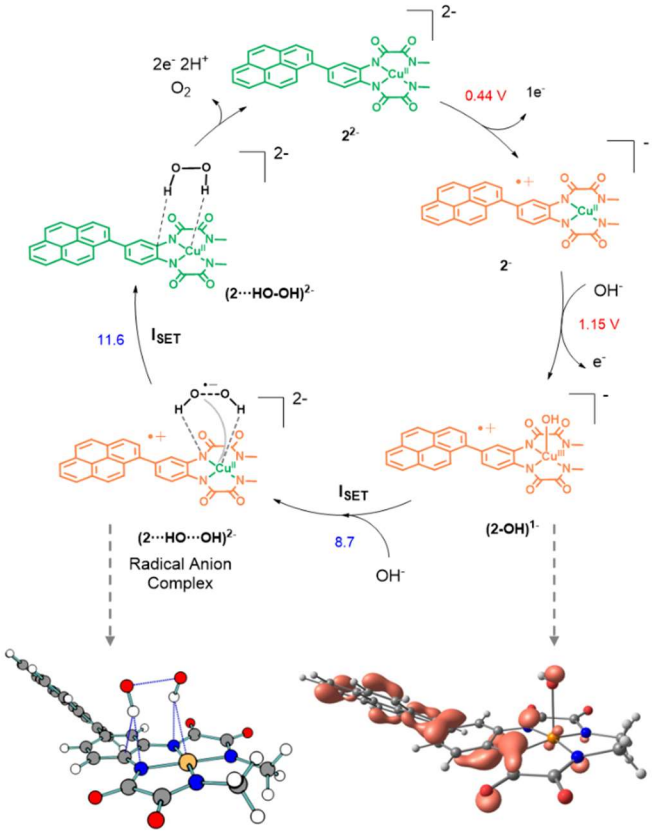

Scheme 1. Computed catalytic cycle for the catalyst $\mathbf{2}^{2-}$. Green color represents the reduced form of the metal center and the ligand while orange color represents their oxidized forms. The values in red refers to calculated oxidation potentials in V and the blue values are free energy in kcal·mol^{-1}.

These are the highest TOF_{max} values ever reported for molecular first row transition metals (Table S4 in SI),[17] demonstrating the importance of electronic delocalization for fast catalysis even in heterogenized complexes.

The stability of the anchored molecular catalysts on grapheme, **G-1**$^{2-}$ and **G-2**$^{2-}$, was analyzed under catalytic turnover by comparing the anodic charge under the first oxidation wave with the charge in the corresponding reduction wave after the electrocatalytic process as shown in the inset of Figure 3C. The comparative analysis showed basically no difference, revealing the high stability of the molecular species in the graphene support. Further evidence for high stability was also obtained by X-ray Absorption Spectroscopy (XAS), as discussed below and further illustrated in Figures 1C-1D, and

by Raman spectroscopy (Figure S35). Both techniques unambiguously show the absence of CuO after catalysis.

A rotating ring disk electrode experiment (RDDE) was carried out for **G-1**$^{2-}$ and **G-2**$^{2-}$ (see Figure S37) to characterize the electrocatalytic generation of oxygen. A Linear Sweep Voltammetry (LSV) was applied in the disk electrode reaching the threshold potential for electrocatalytic water oxidation whereas the ring electrode was set at E_{app} = -0.35 V, for the reduction of the generated dioxygen. The setup yielded Faradaic efficiencies of 23% and 26% for **G-1**$^{2-}$ and **G-2**$^{2-}$, respectively. In addition, a bulk electrolysis experiment was also carried for **G-2**$^{2-}$ deposited on a 1 cm^2 glassy carbon plate as a working electrode and with a Clark electrode placed at the headspace of the electrochemical cell for measurement of the generated dioxygen *in situ* (Figure S33). An applied potential E_{app} = 1.25 V for 20 minutes yielded 0.34 Coulombs and 0.21 μmols of O_2, corresponding to a Faradaic efficiency of 24.5%, similar to the calculated value based on RDDE experiments. The TONs are > 5300 and are the largest ever reported for first row transition metal-based molecular catalysts (See Table S4 in the SI).[17] The low Faradaic efficiency is then likely due to graphene oxidation in parallel to water oxidation reaction in basic solutions.[7] Nevertheless, the molecular catalyst remains intact after catalysis as evidenced by CV and XAS spectroscopy. Indeed, Figure 1C shows that the species after bulk electrolysis are identical to those obtained before catalysis. More important, Figs 1C-1D show that no traces of CuO are revealed by XANES or EXAFS spectra, suggesting that the molecular **G-2**$^{2-}$ active catalyst is robust. This observation is extremely important since most of the molecular catalysts reported so far degrade during the catalytic process yielding the corresponding oxides. This is particularly acute with WOCs based on first row transition metals.[3] Figure 3D shows the catalytic Tafel plots for **1**$^{2-}$, **2**$^{2-}$, **G-1**$^{2-}$ and **G-2**$^{2-}$. It is interesting to observe that the pyrene functionalization of the tetraamide ligand and anchoring to the graphene support has two beneficial effects: decrease the overpotential (η) for catalytic water oxidation by about 200 mV and increases the TOF_{max} by about two orders of magnitude.

In the homogeneous phase, the role of the pyrene group is to stabilize the aromatic ring of the tetraamide moiety via π-delocalization leading to a drastic reduction of the overpotential (η) necessary for catalysis. In the heterogenized **G-1**$^{2-}$ –a complex without a pyrene functionality– π-delocalization is provided by graphene. Interestingly, **G-2**$^{2-}$ exploits the benefit of having both the pyrene moiety and stacking interactions with graphene and end up being the best catalyst. The larger TOF_{max} of **G-2**$^{2-}$ when compared to **G-1**$^{2-}$ suggests that the resulting extended π-delocalization due to pyrene-graphene interactions enhances the ET from the catalyst to the graphene electrode, supporting ET as the rds of the catalytic process.

In conclusion, we have found an extremely rugged and efficient molecular WOC based on Cu, a first-row transition metal complex that is efficient both in the homogeneous phase and heterogenized on graphene electrodes. Importantly, we demonstrated that the molecular catalyst remains intact under catalytic turnover when immobilized on graphene exhibiting no sign of decomposition or formation of CuO during or after catalysis. Furthermore, we found that the pyrene functionality not only acts as a very robust anchoring unit but also facilitates the electrocatalytic oxidation of water to dioxygen both from a thermodynamic and kinetic perspective. Finally, **G-1**$^{2-}$ and **G-2**$^{2-}$ are oxidatively robust hybrid materials with exceptional catalytic performance for water oxidation, rendering them as excellent electroanode candidates for direct solar water-splitting devices.

ASSOCIATED CONTENT

Supporting Information

The Supporting Information is available free of charge on the ACS Publications website. Experimental and additions DFT results.

AUTHOR INFORMATION

Corresponding Author

*victor.batista@yale.edu
*allobet@iciq.cat

Notes

The authors declare no competing financial interests.

ACKNOWLEDGMENT

MINECO, FEDER, ALBA, APS and US DOE. Additional info can be found in the Supporting information.

REFERENCES

(1) Berardi, S.; Drouet, S.; Francas, L.; Gimbert-Surinach, C.; Guttentag, M.; Richmond, C.; Stoll, T.; Llobet, A. *Chem. Soc. Rev.* **2014**, *43*, 7501-7519.

(2) Liu, Y.; Nocera, D. G. *J. Phys. Chem. Commun.* **2014**, *118*, 17060-17066.

(3) Wang, J.-W.; Sahoo, P.; Lu, T.-B. *ACS Catal.* **2016**, *6*, 5062–5068

(4) Karousis, N.; Tagmatarchis, N.; Tasis, D. *Chem. Rev.* **2010**, *110*, 5366-5397.

(5) Alibabaei, L.; Sherman, B. D.; Norris, M. R.; Brennaman, M. K.; Meyer, T. J. *Proc. Natl. Acad. Sci. USA* **2015**, *112*, 5899-5902.

(6) Garrido-Barros, P.; Funes-Ardoiz, I.; Drouet, S.; Benet-Buchholz, J.; Maseras, F.; Llobet, A. *J. Am. Chem. Soc.* **2015**, *137*, 6758–6761.

(7) Hyde, J. T.; Hanson, K.; Vannucci, A. K.; Lapides, A. M.; Alibabaei, L.; Norris, M. R.; Meyer, T. J.; Harrison, D. P. *ACS Appl. Mater. Interfaces* **2015**, *7*, 9554-9562.

(8) DuBois, J. L.; Mukherjee, P.; Collier, A. M.; Mayer, J. M.; Solomon, E. I.; Hedman, B.;Stack, T. D. P.; Hodgson, K. O. *J. Am. Chem. Soc.* **1997**, *119*, 8578-8579.

(9) DuBois, J. L.; Mukherjee, P.; Stack, T. D. P.; Hedman, B.; Solomon, E. I.; Hodgson, K. O. *J. Am. Chem. Soc.* **2000**, *122*, 5775-5787.

(10) Solomon, E. I.; Heppner, D. E.; Johnston, E. M.; Ginsbach, J. W.; Cirera, J.; Qayyum, M.; Kieber-Emmons, M. T.; Kjaergaard, C. H.; Hadt, R. G.; Tian, L. *Chem.Rev.* **2014**, *114*, 3659-3853.

(11) Westre, T. E.; Kennepohl, P.; DeWitt, J. G.; Hedman, B.; Hodgson, K. O.; Solomon, E. I. *J. Am. Chem. Soc.* **1997**, *119*, 6297-6314.

(12) Naqvi, K. R.; Melø, T. B. *Chem. Phys. Lett.* **2006**, *428*, 83-87. Related examples in the literature also show that for the pyrene radical cation the absorption at 420 nm either disappear or suffer a very severe loss of intensity.

(13) Pysh, E. S.; Yang, N. C. *J. Am. Chem. Soc.* **1963**, *85*, 2124–2130. It is important to realize here that the oxidation potential of naphthalene is 700 mV lower than that of benzene. Thus even if the π-delocalization of the pyrene moiety over the phenyl ring of the tetraamdie ligand is small, it will have a very strong impact into the ligand based redox potential.

(14) All redox potentials describe in this paper are referred to the NHE reference electrode.

(15) Costentin, C.; Drouet, S.; Robert, M.; Save´ant, J.-M. *J. Am. Chem. Soc.* **2012**, *134*, 11235-112342.

(16) Matheu, R.; Neudeck, S.; Meyer, F.; Sala, X.; Llobet, A. *ChemSusChem,* **2016**, *9*, 3361–3369.

(17) Blakemore, J. D.; Crabtree, R. H.; Brudvig, G. W. *Chem. Rev.* **2015**, *115*, 12974–13005.

.

Insert Table of Contents artwork here